Progress In Electromagnetics Research, Vol. 113, 179–194, 2011

PHOTONIC CRYSTALS & METAMATERIAL FILTERS BASED ON 2D ARRAYS OF SILICON NANOPILLARS

H. Butt, Q. Dai, and T. D. Wilkinson †

Centre of Molecular Materials for Photonics & Electronics
Department of Engineering, University of Cambridge
9 J. J. Thomson Avenue, Cambridge CB3 0FA, United Kingdom

G. A. J. Amaratunga

Electronics, Power and Energy Conversion Group
Department of Engineering, University of Cambridge
9 J. J. Thomson Avenue, Cambridge CB3 0FA, United Kingdom

Abstract—Highly dense two-dimensional periodic arrays of nano-scaled silicon pillars present interesting photonic band gaps and the capacity to act as photonic crystals which can mould, manipulate and guide light. We demonstrate finite element modelling of silicon pillars based photonic crystals and their effective use in applications like waveguides, optical power dividers, multiplexers and switches. The optical wave propagation through these structures was thoroughly simulated and analysed, confirming their high efficiency. The band gaps studied through the plane wave expansion method are also presented. Later the fabrication of highly periodic two-dimensional arrays of silicon pillars through the process of etching is also explained. The arrays with pillar radius of 50 nm and lattice constant of 400 nm were successfully utilised as photonic crystal waveguides and their measured results are reported. Moreover, the silicon nanopillars sputtered with noble metals can also display artificial optical properties and act as metamaterials due to the mutual plasmonic coupling effects. We report the theoretical results for the silicon nanopillars based metamaterial high-pass filter.

Received 25 December 2010, Accepted 14 January 2011, Scheduled 2 February 2011
Corresponding author: Haider Butt (hb319@cam.ac.uk).
† Haider Butt and Qing Dia contributed equally to this manuscript.

1. INTRODUCTION

Photonic crystals (PCs) are interesting materials which present periodicity in their dielectric constant. Bragg scattering occurs when the periodicity of the dielectric constant is comparable to the wavelength of the incident electromagnetic waves. This introduces band gaps, which means the electromagnetic waves falling in these bands are not able to propagate through the PCs. If these band gaps fall in the optical frequency range they are called photonic band gaps. The band gaps displayed by the PC allow them to effectively influence the light propagation and pave way towards their utilization in various photonic devices [1].

A myriad of research has been conducted on photonic crystal materials and many high refractive index materials have been used for their construction. Silicon (Si), due to its high refractive index and low losses, is one of the extensively used materials of the fabrication of photonic crystals. Recent developments in nanofabrication methods allow us to construct nano-scaled two dimensional arrays of silicon pillars or holes and utilize them as periodic refractive index media for photonic crystals. Numerous studies on the photonic band gaps displayed by 2D arrays of Si pillars have been conducted [2]. The band gaps allow their effective use as waveguides [3, 4], optical switches [5], beam splitters [6], wavelength multiplexers [7], filters, modulators and micro cavities.

Using recent nanofabrication techniques high density 2D arrays of silicon pillars can be fabricated. The arrays with nano-scaled lattice constants a display band gaps well in the range of optical spectrum. We present the modeling and characterization of 2D photonic crystals consisting of Si pillars arrays of radius $r = 50\,\text{nm}$ and lattice constants $a = 400\,\text{nm}$. The band gaps studies were conducted and potential applications presented. Our wave propagation simulation results show the effective use of these photonic crystals in applications like waveguides, optical power dividers, photonic switches and multiplexers. The fabrication and measured results for a Si nanopillars based optical multiplexer are reported.

Likewise, highly dense periodic arrays of Si nanopillars can also be utilized for producing metamaterials. Metamaterials are artificial materials which display material properties not existing in nature. These are composed of sub-wavelength structures fashioned together to exhibit the required values of permittivity and permeability in the desired frequency range. Metamaterials propose myriad interesting applications such as filtering in the terahertz range achieved by using two-dimensional periodic arrays of metallic cylinders [8]. It has been

reported that periodic arrays of thin metal wire structures act as metamaterials and display a cutoff filtering response in the frequency domains depending on the array geometry [9]. These structures demonstrate plasma frequencies which are much lower than in the metal structures and can be utilized for filtering in microwave and terahertz frequency domains [10]. We propose that such metamaterials can be realized by using the metal coated two-dimensional periodic arrays of Si pillars, as metallic nano-wire structures.

The periodic arrays of Si nanopillars, fabricated through the process of etching, present the advantages of being very uniform and defect free, even when fabricated with high material density (having lattice constants of order several hundred nanometers). These characteristics allow them to be effectively used as metamaterial cutoff filters which can operate in the optical domain (unlike the ones previously reported for terahertz frequencies [9]) due to the nanoscale lattice constants. The metallic character required for this application can be achieved by sputtering the arrays with noble metals. Through theoretical calculations we show the operation of an aluminum sputtered Si pillars array, acting as a metamaterial photonic high-pass filter.

2. MODELING OF SILICON BASED PHOTONIC CRYSTALS

2.1. Finite Element Method Simulation

To study the band gap properties of the Si based photonic crystals a finite element simulation method (FEM) was utilized. FEM is an effective computational method for simulating devices consisting of very complex geometries, such as those with nano-scale dimensions. The finite elements used to solve the computational domain can efficiently be concentrated around nanoscale pillars for accurate simulation results. COMSOL Multiphysics [11] is a finite element analysis based software package for modeling of numerous physics and engineering problems. We utilized the *RF Waves* application mode of COMSOL to model the propagation of optical/terahertz waves through the arrays of silicon pillars. Figure 1 shows the geometry of the model established for a 2D square lattice of Si pillars, with a lattice constant a of 400 nm and the pillar radius of 50 nm.

The model represents the bisection of a 2D lattice of infinite vertical rods (Si pillars) in the x-y plane. The medium surrounding the pillars was set to free space by setting the dielectric constant to 1. The dielectric constant for the pillars was set to $\varepsilon = 13 + 0.02i$ [2]. The propagating light was incident on the 2D array from the left of

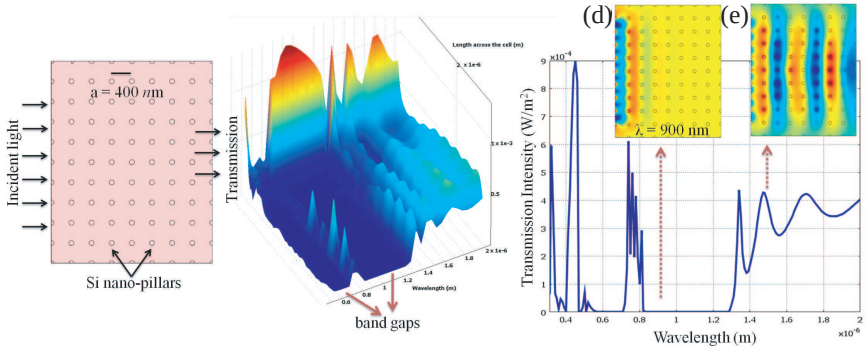

Figure 1. (a) Model geometry of a 2D array of Si pillars, with $a = 400\,\text{nm}$ and $r = 50\,\text{nm}$. (b) The transmission intensity of incident light across the lattice, plotted against wavelength. (c) Cross-section plot of the same. Simulated wave propagation results show two band gaps. Electric field propagation though the lattice of modes having wavelengths of (c) 900 nm and (d) 1500 nm.

the model. The simulations were carried out for the polarization of the incident waves parallel to the axis of the silicon pillars (Transverse Electric (TE) mode). After establishing the shown model geometry as the computational domain the results were computed for wavelengths varying from 400 to 2000 nm, by using COMSOL's inbuilt Parametric SPOOLES solver.

2.2. Band Gaps and Wave Propagation Results

The modeled transmission results are shown in Figure 1(b). The transmission intensity for each wave was plotted across the length of the model cell. The 2D plot of transmission spectra across the cell demonstrates that the lattice presented two band gap regions where no wave propagation took place. The two band gaps ranged from 470 to 710 nm and 830 to 1280 nm. The figure also shows the simulated electric field results for waves with 900 nm and 1500 nm wavelengths. The 900 nm wave is not able to propagate through the lattice due to its belonging to the band gap, unlike the 1500 nm wave which travels through.

The wider band gap of the two is associated with the Bragg condition $\lambda/2 \sim a$, where λ represents the wavelength in the photonic crystal. According to the photonic crystal theory [12], the centre frequency of the band gap is approximately given by the $v \approx c/(2n_{eff}a)$,

where $n_{eff} = \sqrt{(\varepsilon_{eff})}$ is the effective refractive index at low frequencies, $\varepsilon_{eff} = (1 - f) + f^*\varepsilon_r$ is the averaged dielectric permittivity and f is the filling factor of the dielectric (cross-section area of the Si nanopillars/the area of the unit cell). For our lattice $f \approx 0.05$ and the value for the centre frequency determined from the formula above is equal to 1 µm, which matched the simulated results (Figure 1(c)). For the frequency modes with wavelengths bigger than 1.3 µm, the photonic crystal presented a transmission band. The results were in good agreement with the band gaps studies conducted for the arrays of Si pillar using the Plane Wave Expansion (PWE) method.

An array of Si pillars with the same geometry ($a = 400$ nm and $r = 50$ nm) and material properties was modeled using PWE method to calculate the band gaps displayed by the arrays towards the TE-mode waves incident from every direction. The calculated band diagram is shown in Figure 2. In the diagram normalized frequency (on the vertical scale) has been plotted against the incident directions into the lattice (G, X and M as shown in the inset of Figure 2(a)). The normalized frequency $\omega a/2\pi c$, where ω is the angular frequency and c the velocity of light in vacuum, simplifies to a/λ suggesting that the wavelength can be calculated by dividing the lattice constant a with the normalized frequency. The calculations showed that the arrays display two band gaps from 805 to 950 nm ($\omega a/2\pi c = 0.497$–0.421) and from 572.6 to 572.8 nm (0.6985–0.6983). The localization of the two band gaps is consistent with the FEM simulations results however

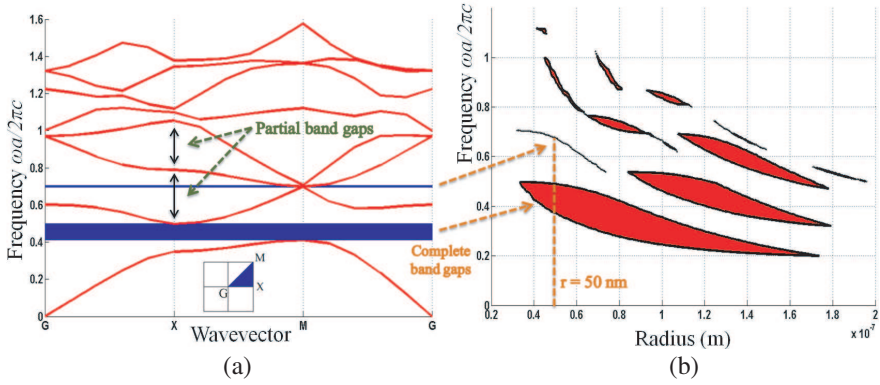

Figure 2. The band diagram for the 2D array of Si pillars, with $a = 400$ nm and $r = 50$ nm. The inset shows the direction of propagation of waves. The band gap map for 2D arrays of Si nanopillars with varying radius and a lattice constant of 400 nm.

the frequency ranges are different. This is because the FEM simulation was performed for only one propagation direction (X) into the lattice, whereas PWE method results present the comprehensive band gaps displayed by the lattice towards the light incident from all possible directions (G, X and M).

The photonic band gaps were also calculated for a range of values for the nanopillar radius r, while a keeping constant value of $a = 400\,\text{nm}$. A photonic band gap map shown in Figure 2(b) displays the possible band gaps areas, where no TE radiation can propagate through the crystal. By following the band gap map the array geometry can be engineered to suit the needs of the optical applications. The widest gap is observed for $r \approx 75\,\text{nm}$ and a normalized center frequency 0.38. A greater number of photonic band gaps can be achieved by increasing the material density of the Si pillars arrays. However, we chose a pillar radius of 50 nm to suit our device applications and capacity of the nanofabrication e-beam technology.

The results were vital as they show that the Si pillars arrays of these dimensions display TE mode band gaps in the optical range and can be utilized for wave guiding and related applications. Within the band gaps no waves are allowed to propagate through the lattice. However, by incorporating defects in the lattice, certain wavelengths belonging to the band gaps can propagate strictly within the defects. The defects can be in the form of line defects to achieve photonic crystal waveguides or point defects producing optical cavities.

2.3. Photonic Crystal Waveguides

By removing a row of Si pillars from the modeled geometry a line defect was introduced in the lattice as shown in Figure 3. The width of the defect was $2a = 800\,\text{nm}$. The wave guiding effects through this defect were studied in detail by simulating the wave propagation through it. The results presented in Figures 3(b)–(d) demonstrate that various frequency modes which were previously forbidden within the band gaps can now propagate through the defect. The waves do not travel out of the defect into the lattice because their frequency lies within the band gap and decay away from the defect. The waves with wavelengths of 550 nm and 950 nm are shown to be guided within the line defect. The result is of interest here as this wave guiding phenomenon can be further utilized for optical switching and wavelength multiplexing at micron-scale.

As the propagation of frequencies belonging to the band gaps is confined within the line defects, line defects with sharp turns can be designed to establish photonic waveguide with sharp turns. To demonstrate this we introduced an L-shaped line defect in the Si

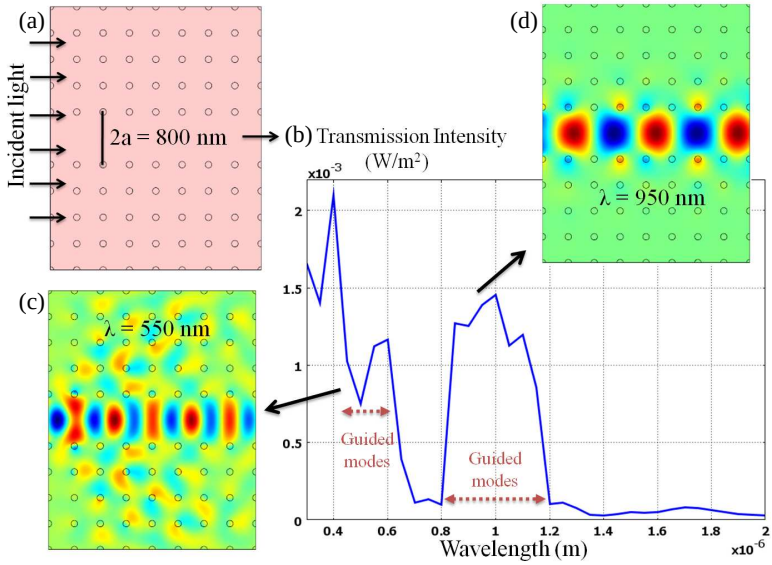

Figure 3. (a) Model geometry of a 2D lattice array of Si pillars with a line defect of width 800 nm (b) The transmission intensity of incident light across the defect, plotted against their wavelength. Simulated electric field intensities of (c) 550 nm and (d) 950 nm waves propagating through the line defect.

pillars lattice and simulated the wave propagation through it. As shown in Figure 4, the frequencies within the band gap do not enter the lattice, except within the line defect and propagate effectively through it despite the sharp turn of 90°. The transmission spectra obtained from two different parts of the lattice are shown in the figure. The spectra obtained from the end of the line 90° turn waveguide shows (Figure 4(c)) the efficient transmission of the frequency modes belonging to the band gaps. However, the spectrum from other part of the lattice (Figure 4(d)) suggest that only the modes belonging to the transmission bands propagate through the lattice.

2.4. Optical Divider and Switches

Having established the photonic crystal waveguides, a variety of passive applications like optical dividers, switches, multiplexers, and ring resonators can be demonstrated by appropriately designing the line defects [13]. In Figure 5(a), we present an efficient optical divider, which divides the propagating optical power equally between the two

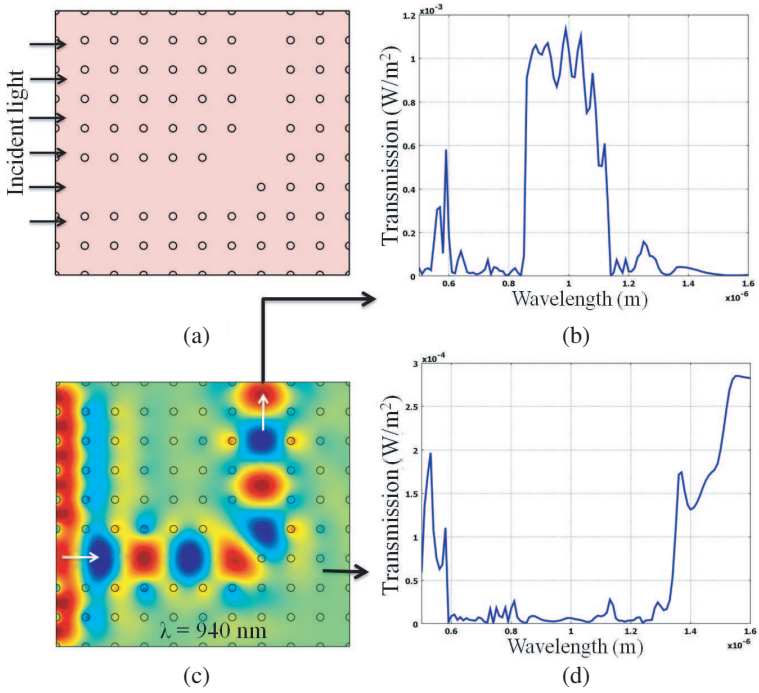

Figure 4. (a) Modeled geometry of a 90 degrees bend photonic crystals waveguide based on arrays of Si pillars. (b) Simulated electric field intensity of a 940 nm wave propagating through that sharp turn waveguide.

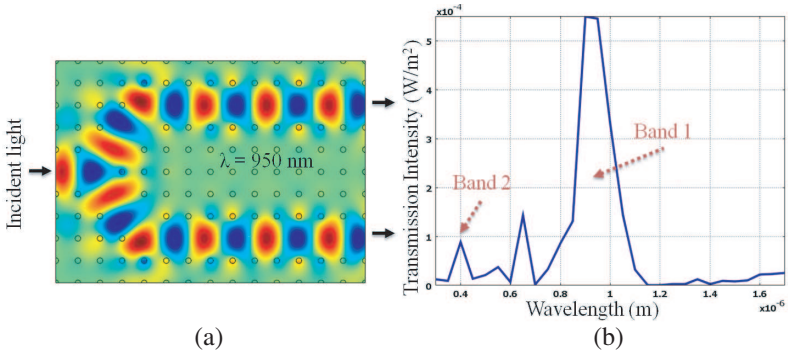

Figure 5. (a) Simulated 950 nm wave propagating through an optical power divider based on 2D array of Si pillars. (b) The calculated transmission spectrum obtained from the ends of the optical power divider. The modes within the band gaps are efficiently transmitted.

branching line defects. The two branching line defects have the same widths; hence, light of 900 nm wavelength can travel through equally. The divider consists of two branching line defects, of widths 850 nm, which transmit the frequency modes belonging to both the band gaps, as observed from the transmission spectrum in Figure 5(b).

Similarly switching of different frequencies in these line defects can be achieved by controlling their widths. In photonic crystals the frequency modes having wavelength comparable to the defect dimensions are able to propagate through them. This concept can be applied by introducing line defects of different dimensions so that different wavelength modes may be guided through them. As shown in Figure 6(b) the geometry of an optical switch which has an input segment branching into two line defects of different widths. The line defect on the top is 850 nm wide, whereas the defect of the bottom is about 640 nm wide. The waves belonging to band gap with wavelengths comparable to the larger defects propagate through as shown in Figures 6(b) and (d). Whereas, the waves belonging to the band gap with shorter wavelengths propagate through the thinner defect at the bottom.

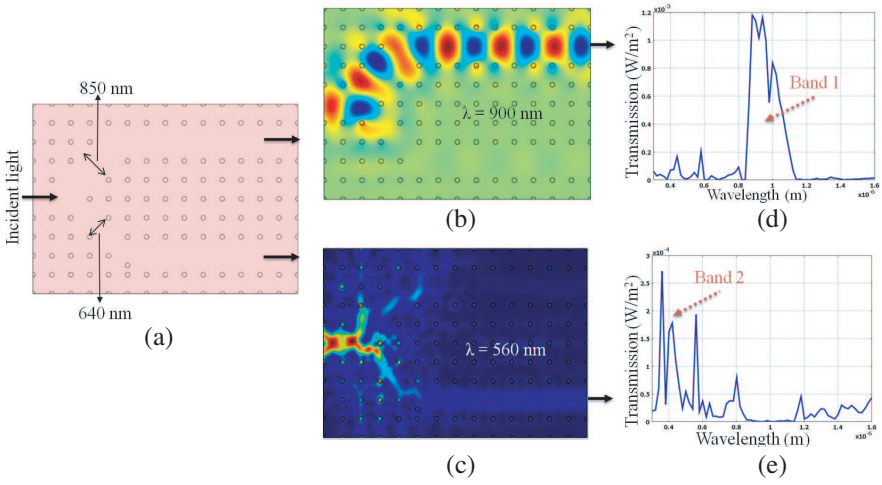

Figure 6. (a) Model geometry for an optical switch with two line defects of different widths. (b) Larger wavelengths like 900 nm propagate through the wider line defect on the top. (c) Transmission intensity plot of a shorter 560 nm wavelength, propagating through the thinner line defect at the bottom. The transmission spectra of waves propagating through the (d) wider and (e) thinner line defects.

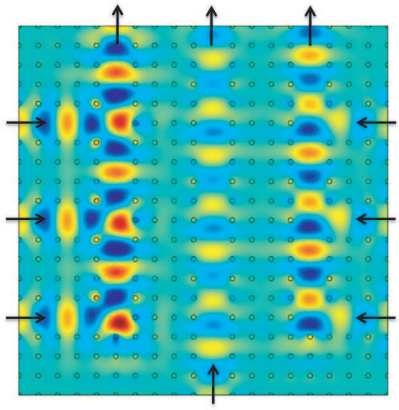

Figure 7. Simulated electric field intensity of a 950 nm wave propagating through an optical multiplexer.

2.5. Wavelength Multiplexing

We also demonstrate the application of wavelength multiplexing utilizing the sharp curved photonic crystal waveguides. The frequency modes within the band gaps can be multiplexed together by branching line defects in 2D arrays of Si pillars, as shown in Figure 7. Different frequency modes can be multiplexed into the common channel through the branching line defects. In this fashion numerous efficiently operating optical applications can be integrated together at micron-scale using photonic crystals.

3. FABRICATION AND CHARACTERISATION

3.1. Fabrication

The fabrication of 2D arrays of silicon pillars was established by first using e-beam lithography to make the dot array pattern (50 nm radius, 400 nm lattice constant) on the Si substrate. The pattern was then sputtered with a metal mask (Tungsten). The process of deep reactive etching (DRIE) was performed for etching the substrate. The array was then exposed to the following gases for a second each, in a succession lasting for 5 minutes: C_4F_8 for protective layering, O_2 for removing the C_4F_8 residues and SF_6 for etching. The final etched substrate was viewed under the scanning electron microscope and well aligned and patterned Si pillars were observed as shown in Figure 8.

The Si pillars lattice was pattered with 800 nm wide line defects producing waveguides with 90° turns. An array of such waveguides

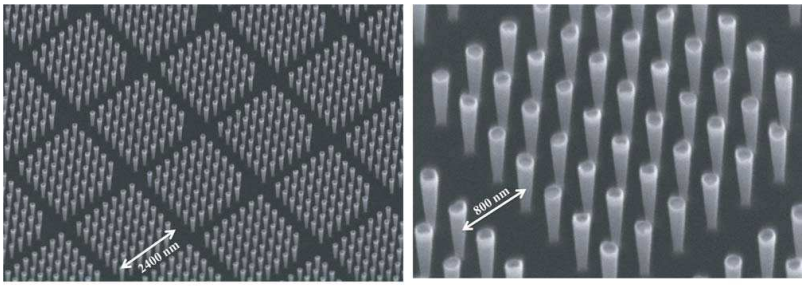

(a) (b)

Figure 8. SEM image of an array of Si pillars with 800 nm wide line defects. Defects are shaped to produce an array of 90° turn waveguides acting as a multiplexer.

was patterned with their ends opening into a common line defect. The device in this arrangement can be utilized as a photonic crystal multiplexer for multiplexing the frequency modes within the band gaps.

3.2. Optical Characterisation Results

The optical characterisation of patterned arrays of Si pillars was carried out. An Ocean Optics 2000 spectrometer was utilized to capture the reflected light from the arrays for the spectral range of almost 450 nm to 1100 nm, with resolution 0.3 nm. Light from a white light source used at an incidence angle of around 60°. The openings of the 90° waveguides were aligned to the incident light beam. The absorption spectra were measured for polarizations of light parallel (TE-transverse electric) and perpendicular (TM-transverse magnetic) to the Si pillars. The light perpendicular to the Si pillars will not be guided through the line defects and was mostly reflected, whereas, the incident light polarized parallel to the pillars was guided within the line defects, due to the band gaps and dips were observed in the reflection spectrum.

Measured reflection spectra for both polarizations of light are presented in Figure 9. In the TM-mode, some strong dips were observed in spectrum corresponding to diffracted light. Waves were not guided through the line defects as the Si pillars do not present a TM-mode photonic band gap. Similar dips were also observed in the TE-mode along with an extra region of increased absorption around 730 to 800 nm which corresponds to the frequency modes that are guided through the waveguides. In our simulations, the TE polarized light was assumed to be incident at an angle of 90° to the Si pillars. However, in experiments an incident angle of near 60° was used due to which the lattice constant offered by the arrays to the incident light

changes and the band gaps shift to smaller wavelengths.

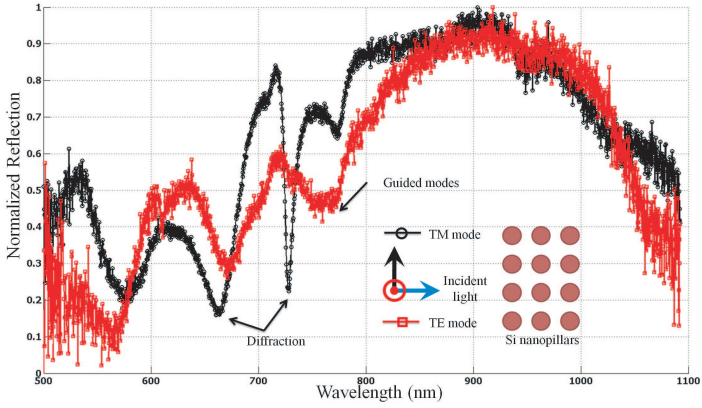

Figure 9. Normalized absorption spectra (TM and TE mode) for an array of sharp turn waveguides based on Si pillar photonic crystals. The light at an incidence angle of 600 was shined on the photonic crystal waveguides.

4. METAMATERIAL HIGH PASS FILTERS

The highly dense periodic arrays of thin Si pillars can also be utilized as metamaterials by sputtering them with noble metals. In this arrangement the arrays display an artificial dielectric function (different from their own) towards the incident light, due to a lower effective plasma frequency of order several hundred terahertz. Pendry et al. [8] demonstrated that the electromagnetic response of a metallic array composed of thin metallic wires, excited by an electric field parallel to the wires (TE-mode) is similar to that of a low-density plasma of very heavy charged particles, with a plasma frequency ω_p:

$$\omega_p^2 = \frac{2\pi c_0^2}{a^2 \ln(a/r)} \tag{1}$$

where c_0 is the velocity of light in vacuum, a is the lattice constant of the 2D wire array, r is the radius of the wires. This concept can be used for lowering the plasma frequency displayed by the metal coated Si pillar arrays achieving negative dielectric constants for metamaterials. The lowering of the plasma frequency is due to the increase in the effective electronic mass within the metallic wires due to the induced current and corresponding magnetic field around them. According to

Eq. (1), the effective plasma frequency strongly depends on the nano-pillar radius and lattice constant. Their values can discretely be chosen to engineer Si pillar arrays of a desired plasma frequency. The resultant frequency dependent permittivity can be calculated using the Drude model for metals described as

$$\varepsilon(\omega) = 1 - \frac{\omega_p^2}{\omega^2} \tag{2}$$

The effective permittivity $\varepsilon(\omega)$ is negative for frequencies less than ω_p, therefore no wave propagation will take place inside the metamaterial. Electromagnetic waves propagation only occurs above ω_p, due to which the structure acts as a nanophotonic high-pass filter [14]. Here we propose that the structure was realized using metal coated square lattice array of Si pillars having radius of 50 nm and lattice constant of 400 nm. Theoretical calculations of the plasma frequency and reflection coefficient of such a nano-scale brush-like array were conducted. For a square lattice of nano-pillar radius 50 nm and lattice constant 400 nm, the plasma frequency $f_p = \omega_p/2\pi$ of 207.5 THz with corresponding plasma wavelength of $\lambda_p = 1.44\,\mu$m were calculated using Eq. (1).

FEM modeling of an array of Si pillars (with $a = 400$ nm and $r = 50$ nm) coated with Aluminum was carried out to confirm the theoretical results. The geometry of the model was similar to the one previously used however the boundary condition for the Si pillars was set to the perfect electric conductor for the purpose of modeling metallic wire arrays. The material properties of the nano-pillars were set to those of Aluminum in the model. The transmission spectra for both TE and TM polarization of light were computed using the model, as shown in Figure 10.

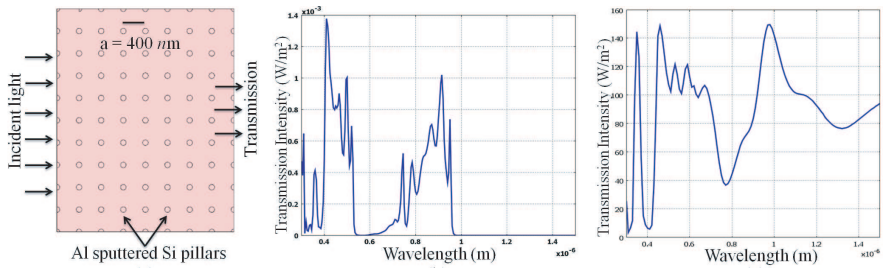

(a) (b) (c)

Figure 10. (a) Model geometry of a 2D array of Al pillars, with $a = 400$ nm and $r = 50$ nm. The calculated transmission spectra for light polarized (b) parallel and (c) perpendicular to the pillars.

It can be observed, the TE-mode spectrum of the metallic photonic crystal presents almost the same alternation of transmission bands and band gaps (near 300 and 600 nm). Till the wavelength of 1 μm the TE-mode spectrum is quite similar to the one displayed by the Si nanopillars, previously shown in Figure 1. However, in the region of larger wavelengths the spectrum exhibits a fundamentally different aspect. Starting from approximately 1 μm, a strong attenuation offered by the lattice, associated with the plasmon-like photonic band, can be observed. The cutoff wavelength of approximately 1 μm numerically calculated from the FEM simulation model is close to the value estimated on the basis of the approximate formula given in Eq. (1) ($\sim$ 1.44 μm). The simulation results agree with the metamaterial theory and after the cut-off frequency no propagation takes place through the lattice. The Al pillars array act as a plasmonic high pass filter, towards the incident waves parallel to the pillars. No such cut-off filtering effect is seen in the TM-mode spectrum (light perpendicular to the pillars), as shown in Figure 10(c). In the TE-mode spectrum (Figure 10(b)) a transmission band is observed just before the cut-off region, whose centre wavelength ($\sim$ 800 nm) corresponds to $\lambda/2 \sim a$. This is reversed as compared to the spectrum of Si nanopillars in Figure 1, where the same relation corresponded to the wider band gap of the two. In this transmission window, the metallic pillars based photonic crystal behave like a group of Fabry-Perot cavities coupled to one another along the propagation direction [12], leading to the corresponding transmission peaks.

Through theoretical results we demonstrate that the sputtered periodic arrays of Si pillars can act as subwavelength wire structures required to establish metamaterials. The fabrication of such arrays

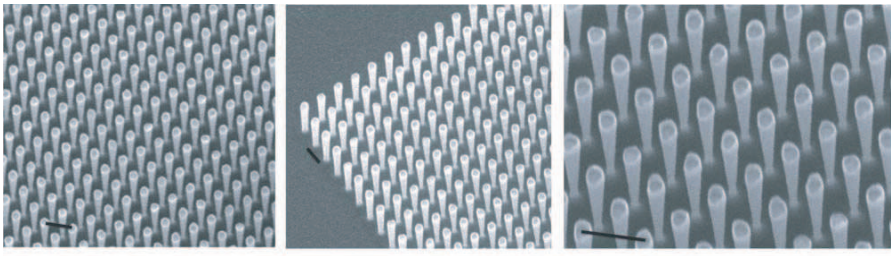

Figure 11. (a) (b) SEM images of 2D periodic arrays of Si nanopillars (with $a = 400$ nm and $r = 50$ nm), which after metal sputtering can act as subwavelength structures in metamaterial filters. (c) The magnified images of the same. The marker represents 400 nm.

was carried out and some SEM images array are shown in Figure 11. Their optical characterization as metamaterial high-pass filter will be reported later. Accordance to Eq. (1), by decreasing the lattice constants of these arrays, their plasmon cut-off frequencies can be brought right in the middle of the optical regime to achieve negative dielectric constant.

5. CONCLUSION

In conclusion, we have presented some interesting applications of photonic crystals based on 2D arrays of silicon pillars. The simulated band gap results were presented for the Si pillars lattice, with a lattice constant of 400 nm and pillar radius of 50 nm. Finite element modeling was utilised to demonstrate the efficient performance of photonic crystals based sharp turn waveguides, optical power dividers, optical switches and multiplexers. The fabrication and optical characterisation of Si pillars based photonic crystal waveguides was performed and good agreement between the two was achieved. We also demonstrated through simulation results that metal sputtered Si pillar arrays can act as subwavelength metallic structures required to establish metamaterial high-pass filters which display cut-off frequencies in the optical regime.

REFERENCES

1. Joannopoulos, J. D., S. G. Johnson, R. D. Meade, and J. N. Winn, *Photonic Crystals: Molding the Flow of Light*, 2nd edition, Princeton University Press, 2008.
2. Poborchii, V. V., T. Tada, and T. Kanayama, "Photonic-band-gap properties of twodimensional lattices of Si nanopillars," *Journal of Applied Physics*, Vol. 91, 3299–3305, 2002.
3. De Dood, M. J. A., E. Snoeks, A. Moroz, and A. Polman, "Design and optimization of 2D photonic crystal waveguides based on silicon," *Optical and Quantum Electronics*, Vol. 34, 145–159, 2002.
4. Zijlstra, T., E. van der Drift, M. J. A. de Dood, E. Snoeks, and A. Polman, "Fabrication of two-dimensional photonic crystal waveguides for 1.5 μm in silicon by deep anisotropic dry etching," *43rd International Conference on Electron, Ion, and Photon Beam Technology and Nanofabrication*, 2734–2739, Marco Island, Florida, USA, 1999.
5. Sharkawy, A., S. Shi, D. Prather, and R. Soref, "Electro-

optical switching using coupled photonic crystal waveguides," *Opt. Express*, Vol. 10, 1048–1059, 2002.

6. Ao, X., L. Liu, L. Wosinski, and S. He, "Polarization beam splitter based on a twodimensional photonic crystal of pillar type," *Applied Physics Letters*, Vol. 89, 171115-3, 2006.
7. Sharkawy, A., S. Shi, and D. W. Prather, "Multichannel wavelength division multiplexing with photonic crystals," *Appl. Opt.*, Vol. 40, 2247–2252, 2001.
8. Pendry, J. B., A. J. Holden, W. J. Stewart, and I. Youngs, "Extremely low frequency plasmons in metallic mesostructures," *Physical Review Letters*, Vol. 76, 4773, 1996.
9. Wu, D., N. Fang, C. Sun, X. Zhang, W. J. Padilla, D. N. Basov, D. R. Smith, and S. Schultz, "Terahertz plasmonic high pass filter," *Applied Physics Letters*, Vol. 83, 201–203, 2003.
10. Gay-Balmaz, P., C. Maccio, and O. J. F. Martin, "Microwire arrays with plasmonic response at microwave frequencies," *Applied Physics Letters*, Vol. 81, 2896–2898, 2002.
11. COMSOL, *COMSOL Multiphysics User's Guide & COMSOL Multiphysics Modeling Guide*, 3.3a edition, 2007, http://www.comsol.com.
12. Lourtioz, J. M. and D. Pagnoux, *Photonic Crystals: Towards Nanoscale Photonic Devices*, Springer, Berlin, 2008.
13. Djavid, M., A. Ghaffari, F. Monifi, and M. S. Abrishamian, "Photonic crystal power dividers using L-shaped bend based on ring resonators," *J. Opt. Soc. Am. B*, Vol. 25, 1231–1235, 2008.
14. Butt, H., Q. Dai, P. Farah, T. Butler, T. D. Wilkinson, J. J. Baumberg, and G. A. J. Amaratunga, "Metamaterial high pass filter based on periodic wire arrays of multiwalled carbon nanotubes," *Applied Physics Letters*, Vol. 97, 163102-3, 2010.